Journal of Metals, Materials and Minerals, 35(1), e2063, 2025

Effects of thickness on the performance of SnO_2 gas sensors using low-temperature co-fired ceramic

Montri AIEMPANAKIT[1], Kittiyaporn SINGSUMPHAN[1], Chutima NAKMUK[1], Cheewita SUWANCHAWALIT[2], Manatsawee SRIRAK[3], Kata JARUWONGRUNGSEE[3], Anurat WISITSORAAT[4], Monrudee LIANGRUKSA[5], and Chawarat SIRIWONG[1,*]

[1] *Department of Physics, Faculty of Science, Silpakorn University, Nakhon Pathom, 73000 Thailand*
[2] *Department of Chemistry, Faculty of Science, Silpakorn University, Nakhon Pathom, 73000 Thailand*
[3] *Opto-Electrochemical Sensing Research Team (OEC), National Electronics and Computer Technology Center (NECTEC), National Science and Technology Development Agency (NSTDA), Pathum Thani, 12120 Thailand*
[4] *National Security and Dual-Use Technology Center (NSD), National Science and Technology Development Agency (NSTDA), Pathum Thani, 12120 Thailand*
[5] *National Nanotechnology Center (NANOTEC), National Science and Technology Development Agency (NSTDA), Pathum Thani 12120, Thailand*

***Corresponding author e-mail:** first_164@hotmail.com

Received date:
22 May 2024
Revised date:
6 December 2024
Accepted date:
5 Fabruary 2025

Keywords:
SnO_2 nanoparticles;
Gas sensors;
Ethanol detection;
Low-temperature co-fired ceramic (LTCC);
Low-power sensing

Abstract

This study develops SnO_2-based gas sensors integrated with a low-temperature co-fired ceramic (LTCC) micro hotplate for ethanol detection. SnO_2 nanoparticles were synthesized using a simple precipitation method, and sensing layers with varying thicknesses around 0.24 µm, 0.71 µm, and 1.20 µm were applied to evaluate their influence on performance. The results show that the optimal configuration is a 0.71 µm layer, offering high sensitivity, fast response, and efficient recovery. Operating at a low voltage of 3.2 V, the sensors exhibit low power consumption, suitable for portable and battery-operated applications. The gas-sensing mechanism relies on changes in resistance due to interactions between ethanol molecules and oxygen species adsorbed on the SnO_2 surface, with the optimal sensor showing superior selectivity for ethanol (C_2H_5OH) over other gases, including hydrogen sulfide (H_2S), ammonia (NH_3), acetone (C_3H_6O), and nitric oxide (NO). The structural and electrical properties of the SnO_2 layers, combined with the efficiency of the LTCC micro hotplate platform, contribute to stable sensing performance. This research highlights the importance of thickness optimization to balance sensitivity and response. The proposed sensor offers a low-cost, energy-efficient solution for ethanol monitoring, with potential enhancements through material doping, multi-gas detection, and IoT integration.

1. Introduction

Gas sensors are essential in detecting and measuring gases or vapors across diverse environments. Their applications range from industrial settings, where gas is a primary operational component to enclosed spaces. The ability to detect hazardous gases, leaks, vapors, or smoke is crucial for reducing the risk of accidents. Additionally, gas sensors are needed in production control, ensuring product quality and preventing damage during industrial processes [1-3]. Among the many gases and vapors that require precise monitoring, ethanol (C_2H_5OH) stands out due to its widespread use across several industries. Ethanol is vital in alcoholic beverage production, pharmaceuticals, medical applications, and biofuels. However, ethanol's volatility poses significant safety risks, as exposure to high concentrations can affect human health and increase the potential for accidents. Thus, developing gas sensors capable of accurately detecting ethanol is critical for improving safety and operational efficiency in various applications [2,4]. Low-temperature co-fired Ceramic (LTCC) technology facilitates the rapid, energy-efficient production of gas sensors that are also resistant to harsh environments. LTCC allows the integration of electronic circuits and heating elements on a single ceramic substrate, making it ideal for portable, battery-operated devices. The reduced power consumption achieved with LTCC technology is particularly beneficial for sensors used in remote monitoring or wearable applications [5,6]. Metal oxide semiconductors (MOS) are widely used in gas sensors due to their high sensitivity, accuracy, and low production costs. Among these, tin dioxide (SnO_2) is a promising candidate, featuring a band gap of approximately 3.6 eV, which allows it to detect gases such as hydrogen [7], carbon monoxide [8], and volatile organic compounds (VOCs) [9], including ethanol [10-12].

Several studies have utilized LTCC technology combined with SnO_2 to develop gas sensors for various applications. For instance, Kulhari *et al*. developed an LTCC-based SnO_2 sensor for detecting carbon monoxide (CO), focusing on reducing power consumption

while maintaining high sensitivity. However, their sensor required elevated temperatures for optimal performance, which increased overall energy usage [6]. Similarly, Rydosz *et al*. investigated using LTCC platforms with SnO_2 for various gas detection applications, emphasizing thermal and electrical optimization but still relying on higher operating temperatures that may limit energy efficiency [13]. While these studies highlight the potential of LTCC and SnO_2 integration, they often require significant material usage or operate at higher energy levels than desired for portable applications.

This research differs significantly by emphasizing extremely low power consumption, compactness, and portability. The sensor developed in this study utilizes a minimal amount of SnO_2, as the gas-sensing component is integrated into an LTCC micro hotplate platform smaller than a human hair. This miniaturized design not only reduces material usage but also enables efficient and reliable gas detection in portable devices. However, the performance of SnO_2-based gas sensors depends heavily on factors such as the thickness of the sensing layer and temperature control. Increasing the thickness of the sensing material enhances the surface area, improving the sensor's response. Excessive thickness may introduce challenges like slower response times and signal attenuation. Therefore, optimizing the thickness of the sensing material is essential to developing efficient gas sensors [14,15]. This research focuses on developing a gas sensor using SnO_2 as the primary sensing material integrated into an LTCC micro hotplate platform. The study investigates how the thickness of the sensing layer influences ethanol detection performance. Key parameters such as response value, sensitivity, response time, recovery time, and selectivity toward different gases are analyzed. The ultimate goal is to create a high-performance, energy-efficient gas sensor tailored to detect ethanol effectively, with the potential for broader applications in other industries that require precise gas detection.

2. Experimental section

2.1 SnO_2 nanoparticle

2.1.1 Synthesis of SnO_2 nanoparticles

SnO_2 nanoparticles were synthesized using a modified precipitation method based on the procedures described by Paulraj *et al.*and Horti *et al.* [16,17]. The synthesis involves preparing a solution by mixing 100 mL of deionized (DI) water with 2.256 g of $SnCl_2{\cdot}2H_2O$ in a suitable container. Stir the solution continuously for 5 min to ensure complete dissolution. Adjust the pH of the solution to 10 by slowly adding 0.5 M NaOH solution under continuous stirring. After adjusting the pH, maintain stirring for an additional 3 h to facilitate the precipitation of SnO_2 nanoparticles. Filter the precipitate and wash it with ethanol and DI water several times to remove any residual chloride ions. Transfer the purified precipitate into a centrifuge tube and centrifuge it to separate the solid particles from the liquid phase. Discard the supernatant, and repeat the washing and centrifugation steps several times to ensure complete purification.

After purification, transfer the precipitate to a suitable container and dry it in a hot air oven at 80°C for 24 h. The dried nanoparticles are then annealed in a high-temperature furnace at 500°C for 3 h to improve their crystallinity. The entire synthesis process is summarized in Figure 1.

2.1.2 Characterizations

The structural properties and morphology of SnO_2 nanoparticles were analyzed using X-ray diffraction (XRD) measurements performed on PANalytical Aris systems with CuK_α radiation (λ = 1.540598 Å). The sample morphology was examined using Field emission Scanning electron microscopy (FE-SEM, TESCAN MIRA 3) and Transmission electron microscopy (TEM, Philips TECNAI 20). FE-SEM was equipped with energy-dispersive X-ray spectroscopy to analyze the chemical composition. The functional groups of the sample were identified using Fourier transform infrared spectroscopy (FT-IR, Perkin Elmer Spectrum 100).

2.2 Sensing device preparation

The LTCC micro hotplate used in this research follows the designs described in Thai patents No. 2301005878 (2023) from the National Electronics and Computer Technology Center NECTEC), detailing the micro-hotplate's structure and signal analysis techniques. This micro hotplate features a bridge-type configuration with double-sided patterning. The top surface contains interdigitated electrodes for measuring changes in the electrical properties of the gas-sensing material in contrast, the bottom surface holds a meander-shaped micro-heater to regulate the operating temperature. The bridge structure, 130 µm wide, ensures efficient thermal isolation and minimizes power consumption during operation. The interdigitated electrodes have specific dimensions: the total spacing between two adjacent electrodes (L_c) is 15 µm, the gap spacing between electrodes (L_s) is 6 µm, and the length of the parallel electrodes (L_f) is 200 µm. This design enables the hotplate to achieve temperatures exceeding 400°C with a heating power of approximately 70 mW, making it ideal for portable, low-power applications [18].

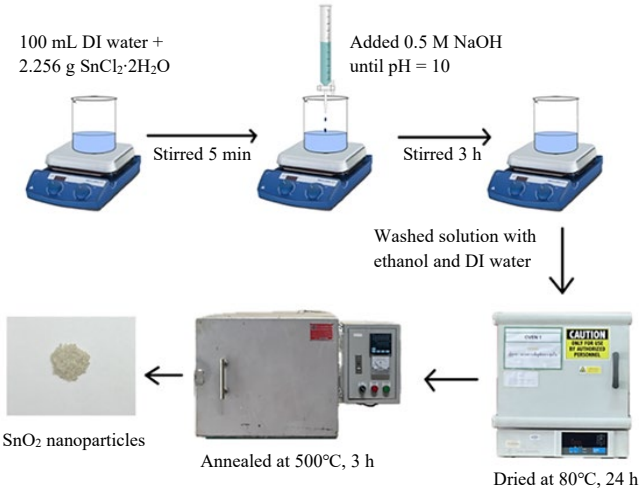

Figure 1. Schematic representation of synthesis process of SnO_2 nanoparticles using precipitation technique.

To fabricate the sensing device, a binder solution was first prepared by mixing 18 g of alpha-terpineol with 430 mL of ethyl cellulose and stirring the mixture at 80°C for 6 h. After cooling, 30 mg of SnO_2 powder was combined with 150 µL of the prepared binder solution and ground for 30 min to ensure a homogeneous paste. The resulting SnO_2 paste was then applied onto the LTCC micro hotplate and dried at 100°C for 5 min. Multiple layers were added: one layer (SnO_2-1), two layers (SnO_2-2), and three layers (SnO_2-3) to explore how varying the thickness of the sensing material affects the sensor's gas detection performance. Each sample was annealed at 450°C for 2 h after the final layer was applied to stabilize the SnO_2 films. The goal of varying thickness was to determine whether the increased surface area would enhance or hinder the sensor's ability to detect different gases.

At this stage, the sensor's selectivity toward specific gases was not predetermined. Instead, the focus was on observing how thickness influences performance metrics such as response time, sensitivity, and recovery time. Subsequent tests will expose the sensors to various gases, including ethanol, to assess their performance and identify the optimal thickness configuration. This approach ensures a systematic investigation into the relationship between film thickness and gas detection efficiency, which is critical for optimizing sensor design for practical applications.

2.3 Gas sensing measurement

The prepared SnO_2-coated LTCC micro hotplate samples were placed in a gas chamber for sensing measurements, as shown in Figure 3. A mass flow controller (MFC) was used to regulate the concentration of test gases, ensuring precise mixing with dry air for concentration control. The target gases selected for the study were H_2S, NH_3, C_3H_6O, NO, and C_2H_5OH, with concentrations ranging from 2 ppm to 100 ppm. During the tests, the supply voltage was varied between 2.0 V and 3.6 V, and the data were continuously monitored and collected via a computer interface, as illustrated in Figure 3.

The sensor response was determined by measuring the change in resistance of the SnO_2-coated LTCC micro hotplate upon exposure to the target gases. The sensor response (S) is defined using the following formula:

$$S = R_a/R_g \quad (1)$$

Where R_a is the resistance in dry air and R_g is the resistance in the presence of the target gas [19].

This response value reflects the change in conductivity caused by interactions between the target gas and the SnO_2 sensing layer. The SnO_2 surface adsorbs oxygen species in dry air, forming negatively charged ions that increase resistance by reducing free electrons. When exposed to the target gases, these oxygen species react with the gas molecules, releasing electrons into the conduction band and decreasing resistance. By calculating the ratio of R_a to R_g, the sensor's sensitivity to each gas is quantified, allowing for a comprehensive evaluation of its performance.

The results from these measurements are crucial for understanding the sensor's behavior, particularly its sensitivity, selectivity, and response dynamics under different gas concentrations and operating voltages.

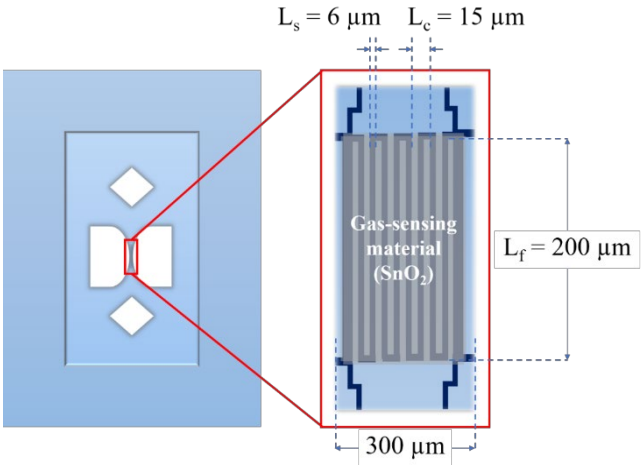

Figure 2. Schematic representation of SnO_2-based gas sensor fabricated on LTCC substrate.

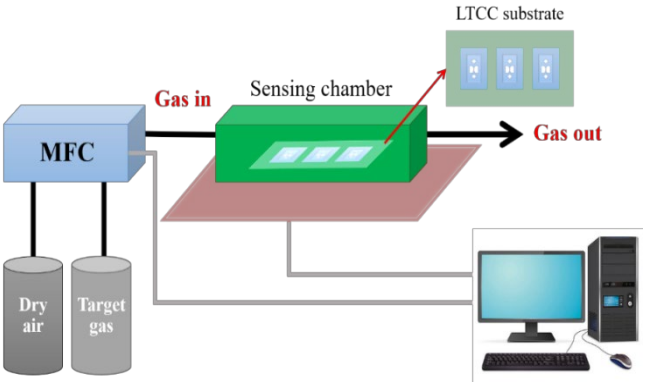

Figure 3. Schematic diagram of gas sensing analysis and the inset image in the sensing chamber shows the LTCC micro hotplate used for gas sensing applications.

3. Results and discussion

3.1 Characterization of SnO_2 nanoparticles

3.1.1 XRD Analysis

The X-ray diffraction (XRD) pattern of the synthesized SnO_2 nanoparticles, shown in Figure 4, confirms the material's crystal structure and phase purity. The prominent peaks appear at 2θ values of 26.6°, 34.0°, 38.0°, 51.8°, 54.8°, 57.9°, 61.9°, 64.6°, 66.0°, 71.3°, and 78.7°, corresponding to the crystal planes (110), (101), (200), (211), (220), (002), (310), (112), (301), (202), and (321), respectively. These peaks agree with the standard pattern for rutile-type tetragonal SnO_2 (JCPDS No. 41-1445) [20,21], confirming the successful synthesis of the desired phase without any detectable impurities or secondary phases.

The well-defined peaks with high intensity indicate good crystallinity, suggesting the nanoparticles have a stable and ordered structure. This structural stability is essential for maintaining consistent gas-sensing performance. Furthermore, the absence of any additional peaks in the XRD pattern confirms the high purity of the SnO_2 sample, ensuring that no unintended by-products were formed during the synthesis.

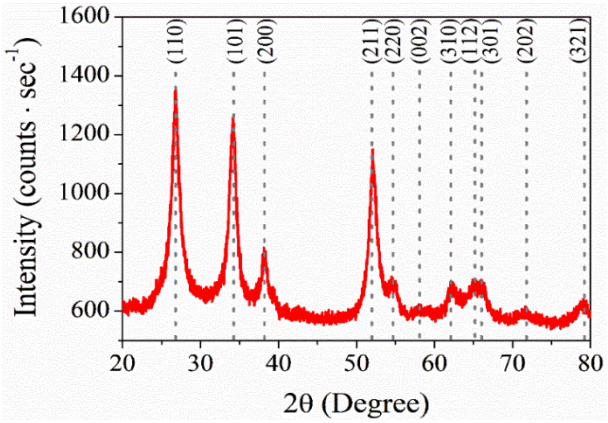

Figure 4. XRD pattern of the SnO_2 nanoparticle.

3.1.2 FE-SEM and EDS Analysis

The morphology and elemental composition of the synthesized SnO_2 nanoparticles were investigated using Field emission scanning electron microscopy (FE-SEM) and energy-dispersive X-ray spectroscopy (EDS). The FE-SEM images, shown in Figure 5, reveal that the SnO_2 nanoparticles exhibit a quasi-spherical morphology with minimal agglomeration. The particle surfaces appear smooth, and the nanoparticles are evenly distributed, suggesting uniform synthesis. The size observed from the FE-SEM images correlates well with the average particle size determined from TEM analysis, approximately 13.7 ± 0.3 nm.

The EDS spectrum, presented in Figure 5, confirms the elemental composition of the SnO_2 nanoparticles. The spectrum shows strong peaks corresponding to tin (Sn) and oxygen (O), with no detectable impurities, further validating the high purity of the synthesized material. The quantitative analysis from EDS, indicates that the weight percentages of Sn and O are 83.2% and 16.8%, respectively, while their atomic percentages are 39.9% and 60.1%, respectively. These results align with the expected stoichiometry for SnO_2, confirming the successful synthesis of tin dioxide.

3.1.3 TEM Analysis

The TEM analysis of the synthesized SnO_2 nanoparticles reveals a quasi-spherical morphology with slight agglomeration. The average particle size, calculated from 100 measurements, is 13.7 ± 0.3 nm. This consistent particle size distribution confirms the reproducibility of the synthesis process, as shown in Figure 6. The uniform size contributes to the stability of the sensing material, ensuring reliable performance across different sensor samples.

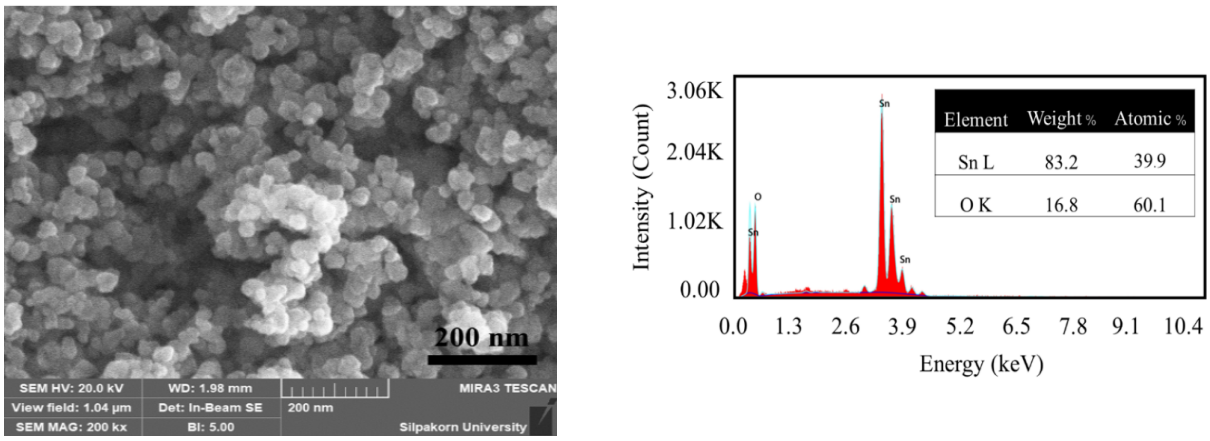

Figure 5. FE-SEM image and EDS spectrum of the synthesized SnO_2 nanoparticles.

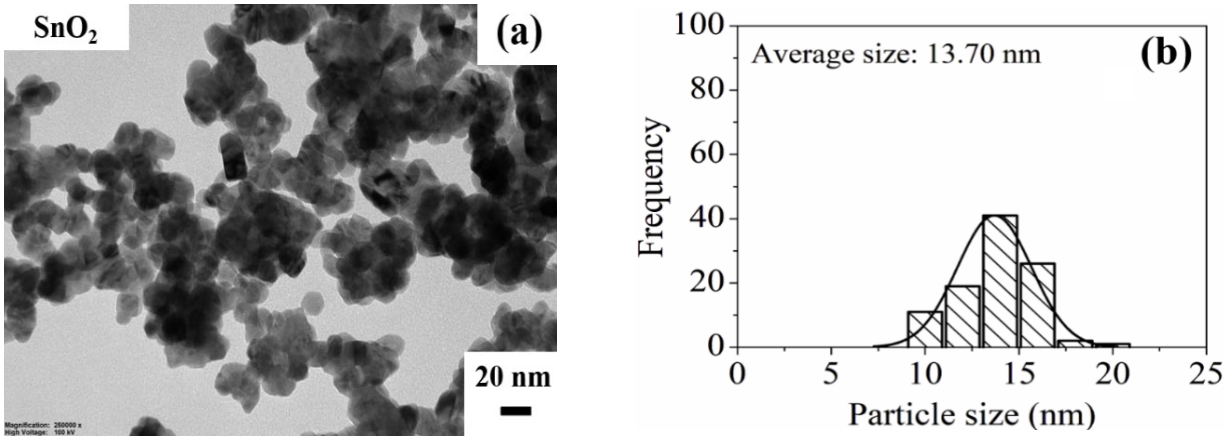

Figure 6. (a) TEM images and particle size distribution of the synthesized SnO_2 nanoparticles using the precipitation method, (b) Particle size distribution (n = 100) of SnO_2 nanoparticles indicates the average size of 13.70 nm.

3.1.4 FT-IR Analysis

The FT-IR spectrum of the synthesized SnO_2 nanoparticles, presented in Figure 7, shows a single prominent peak at 596 cm^{-1}, corresponding to the Sn–O stretching vibration. This peak confirms the presence of tin oxide and indicates that the material was successfully synthesized with the expected metal-oxide bonding [22]. The clarity of this peak suggests high purity, as no significant interfering peaks from residual organic compounds or synthesis by-products were detected.

Although only one evident Sn–O peak is observed, minor baseline variations near 3400 cm^{-1} and 1630 cm^{-1} may indicate trace amounts of adsorbed moisture or hydroxyl groups, commonly found on metal oxides' surfaces due to environmental exposure. These hydroxyl groups, if present, could enhance surface reactivity and contribute to the gas adsorption mechanism during sensing operations [23].

3.1.5 Band Gap Analysis

The band gap energy of the synthesized SnO_2 nanoparticles was estimated using UV-Vis spectroscopy and analyzed through the Tauc plot method, which relates the absorption coefficient to photon energy. The Tauc relation is expressed as:

$$(\alpha h\nu)^n = A(h\nu - E_g) \quad (2)$$

where α is absorption coefficient, $h\nu$ is photon energy, E_g is band gap energy, A is constant, n is exponent (for direct band gap materials like SnO_2, ($n = 2$) [24].

In this method, the photon energy $h\nu$ is plotted against $(\alpha h\nu)^2$, and the linear region of the plot is extrapolated to intersect the x-axis, where $(\alpha h\nu)^2 = 0$. The band gap energy, determined from Figure 8, is 3.64 eV, which aligns with the typical range for SnO_2 [25-27]. This wide band gap limits intrinsic conductivity at room temperature but allows for enhanced conductivity at elevated temperatures through the thermal excitation of electrons across the band gap. As a result, the sensor operates more effectively at higher temperatures, making it suitable for gas-sensing applications. [8,28,29].

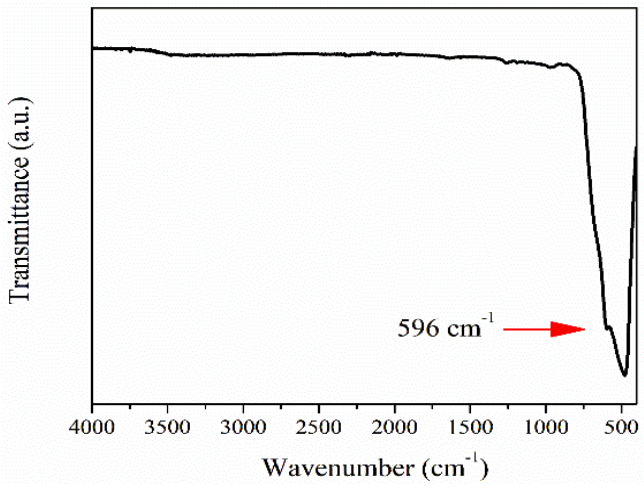

Figure 7. FT-IR spectra of the synthesized SnO_2 nanoparticles prepared by the precipitation method.

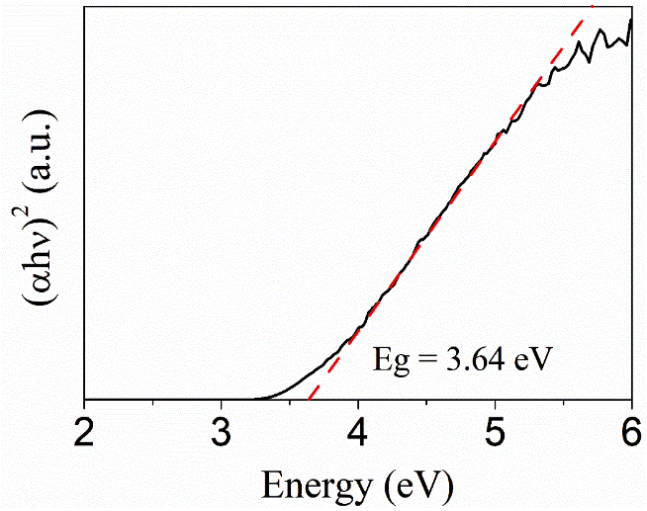

Figure 8. Band gap energy estimation from the Tauc plot of the synthesized SnO_2.

3.2 Thickness of gas-sensing material on LTCC micro hotplate

The thickness of the SnO_2 gas-sensing layers applied on the LTCC micro hotplate was measured using cross-sectional FE-SEM images. The results indicate that the thicknesses of the single-, double-, and triple-layer coatings are 0.24 ± 0.02 µm, 0.71 ± 0.03 µm, and 1.20 ± 0.05 µm, respectively. These measurements confirm the uniformity of the coating process, with each additional layer contributing predictably to the overall thickness. All samples were annealed at 450°C for 2 h to ensure proper adhesion to the LTCC substrate and structural stability.

The FE-SEM images, as shown in Figure 9, reveal a porous surface morphology across all SnO_2 layers. This porosity plays a critical role in gas sensing, as it enhances the surface area available for gas adsorption, which is expected to improve the sensor's sensitivity. However, as the layer thickness increases, inevitable trade-offs may arise. While thicker layers can increase the capacity for gas adsorption, they may also introduce higher internal resistance due to electron scattering, potentially reducing the speed of response and recovery. Conversely, thinner layers might allow for faster electron transport but may exhibit reduced sensitivity due to the smaller surface area available for interaction with gas molecules.

These observations suggest that the gas detection performance depends on finding the optimal thickness and balancing sensitivity with efficient electron transport. The next section presents the gas detection measurements and explore how these thickness variations influence the sensor's performance, including sensitivity, response time, recovery time, and selectivity.

3.3 Gas-sensing properties and mechanisms

This section presents the gas detection measurements performed with the SnO_2 sensors at different thicknesses and explains the underlying mechanisms that govern their response. Key performance metrics, including sensitivity, response time, recovery time, and selectivity, were evaluated, along with insights into the role of surface interactions and electron transport in gas sensing.

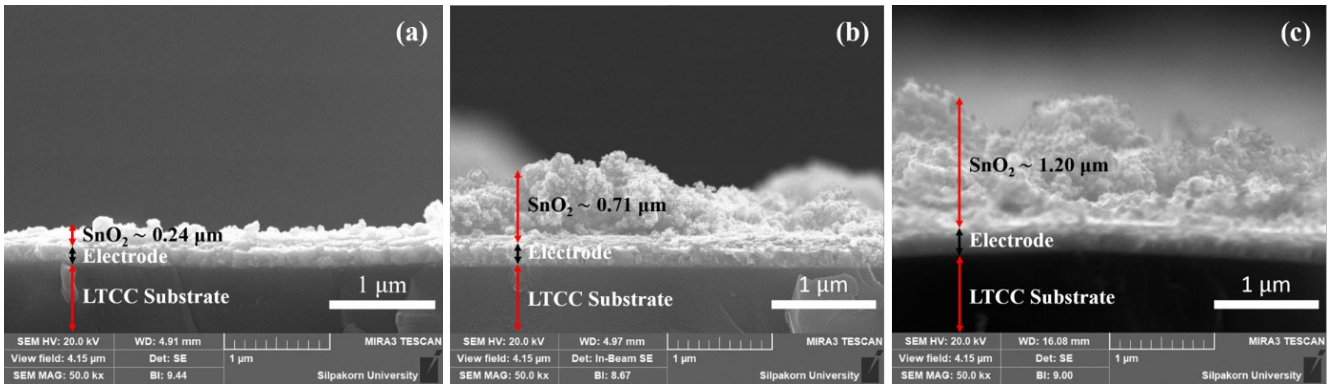

Figure 9. FE-SEM cross-section image. The thickness of gas-sensing material on the LTCC micro hotplate of the sample (a) SnO_2-1, (b) SnO_2-2, and (c) SnO_2-3, respectively.

3.3.1 Measurement of sensor response

The SnO_2 sensors were exposed to ethanol concentrations ranging from 2 ppm to 100 ppm, with real-time resistance changes recorded. Each test was repeated three times in Figure 10(b-f), indicating the standard deviation from these independent measurements.

3.3.2 Effect of thickness on gas sensing

The dynamic response of the sensors with thicknesses of 0.24 µm, 0.71 µm, and 1.20 µm to ethanol is shown in Figure 10(a). The 0.71 µm layer exhibited the best overall performance, combining high sensitivity and fast response and recovery times. In contrast, the thicker 1.20 µm layer showed slower response and recovery times due to increased electron scattering and higher internal resistance, which hindered charge carrier mobility. Meanwhile, the thinner 0.24 µm layer responded quickly but exhibited lower sensitivity due to its reduced surface area for gas adsorption.

The sensor response increased linearly with ethanol concentration, as illustrated in Figure 10(b), particularly for the 0.71 µm sensor. This confirms that increasing the surface area by adjusting the thickness to an optimal point enhances sensitivity. Figure 10(c-d) demonstrate the effect of thickness on response time and recovery time. The 0.71 µm layer achieved a response time of 2 s and exhibited a shorter recovery time than the 1.20 µm layer, which was slowed down by higher resistance.

3.3.3 Selectivity and voltage optimization

To assess their selectivity, the sensors were tested with various gases, including H_2S, NH_3, C_3H_6O, NO, and C_2H_5OH. Figure 10(f) shows that the sensors exhibited superior selectivity toward ethanol over other VOCs. This selective response is attributed to ethanol's surface interaction energy and reaction kinetics with SnO_2, as ethanol molecules interact more favorably with the oxygen ions adsorbed on the sensor's surface, releasing electrons back into the conduction band.

The effect of voltage on sensor performance was analyzed, as shown in Figure 10(e). The sensors performed optimally at 3.2 V, where the 0.71 µm layer achieved the highest response. Increasing the voltage beyond this point did not significantly improve performance, confirming that the sensor operates efficiently with low power consumption.

3.3.4 Gas-sensing mechanisms

The gas-sensing mechanism of SnO_2 sensors relies on changes in electrical resistance driven by surface interactions with gases. Figure 11 provides a schematic representation of these mechanisms. When exposed to air, oxygen molecules (O_2) adsorb onto the SnO_2 surface and capture electrons from the conduction band, forming negatively charged oxygen species (O_2^-, O^-, and O^{2-}):

$$O_2(\text{gas}) + e^- \rightarrow O_2^-(\text{absorbed}) \quad (3)$$

This process increases the sensor's resistance by reducing the number of free electrons available for conduction. Upon exposure to ethanol, the gas molecule react with the adsorbed oxygen species, releasing electrons back into the conduction band and reducing the sensor's resistance:

$$C_2H_5OH + 3O^- \rightarrow 2CO_2 + 3H_2O + 3e^- \quad (4)$$

This release of electrons results in a measurable drop in resistance, which forms the basis of the sensor's response to ethanol [30]. Figure 11(b) illustrates this reduction in resistance when ethanol is present, highlighting how the sensing layer facilitates rapid adsorption and desorption cycles essential for gas detection.

The gas-sensing performance of SnO_2 sensors depends critically on the thickness of the sensing layer, with the 0.71 µm layer providing optimal results. This configuration balances high sensitivity, fast response times, and efficient recovery, ensuring reliable performance with low power consumption (See Figure 10). The sensor's selective response to ethanol over other VOCs is driven by favorable surface reactions, which enhance electron transport and conductivity changes. The gas-sensing mechanisms illustrated in Figure 11 further explain how the adsorption and reaction of gases with oxygen species on the SnO_2 surface control the sensor's resistance, enabling accurate detection of ethanol and other gases.

Table 1 provides a comparative overview of the ethanol sensing performance of various SnO_2-based materials reported in the literature, compared with the results from this study. The comparison highlights vital parameters, including operating temperature, ethanol concentration (ppm), and sensor response (R_a/R_g), which is the ratio of resistance in air (R_a) to resistance in ethanol (R_g). The sensors in the table utilize

various structural modifications such as doping, nanospheres, hollow structures, and composites, with operating temperatures ranging from 150°C to 350°C. While many of these sensors achieve high responses, they require elevated temperatures, leading to higher power consumption.

In contrast, the SnO_2 sensor developed in this study achieves the highest response (R_a/R_g = 74) for 100 ppm ethanol among the listed works, without relying on such high temperatures. The sensor operates efficiently at a low supply voltage of 3.2 V, which, based on the findings from L. Kulhari *et al.* [6], corresponds approximately to a temperature of 250°C to 280°C for similar LTCC micro hotplates. This highlights the advantages of the low-power LTCC platform, which supports energy-efficient gas sensing while maintaining excellent sensitivity.

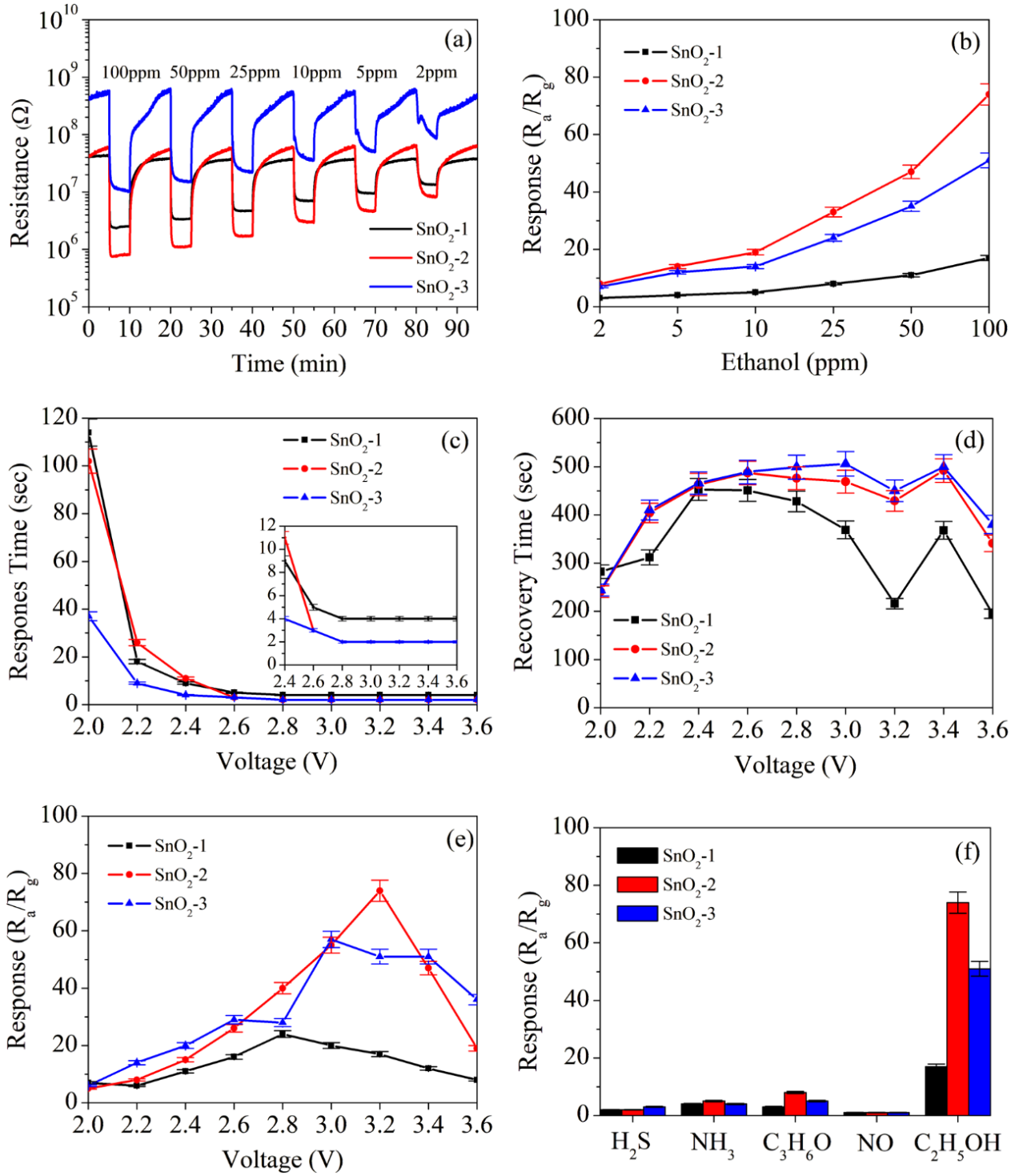

Figure 10. The effects of sensing layer thickness on gas-sensing performance. (a) Dynamic responses of SnO_2 sensors with different thicknesses (0.24 µm, 0.71 µm, 1.20 µm) to varying ethanol concentrations, (b) The linear relationship between response and ethanol concentration. Error bars represent the standard deviation from three independent measurements, (c) Response times for each thickness at 3.2 V, with the 0.71 µm layer showing the fastest response (2 s), (d) Recovery times, with thicker layers recovering more slowly due to higher resistance, (e) Sensor response at 100 ppm ethanol under different voltages, identifying 3.2 V as the optimal voltage, and (f) Selectivity of sensors toward various gases, showing higher sensitivity to ethanol.

Table 1. Ethanol sensing properties of various SnO_2-based materials.

Material	Temperature [°C]	Ethanol [ppm]	Response (R_a/R_g)	Ref.
ZnO-doped porous SnO_2 hollow nanospheres	150	100	14.8	[31]
SnO_2 hollow microspheres	320	100	33	[32]
Reduced graphene oxide appended SnO_2 hollow nanoparticles	300	100	70	[33]
nanosheets-assembled SnO_2 hollow spheres	350	100	11	[34]
SnO_2 hollow spheres	250	100	46	[35]
Hollow Pentagonal Cone-Structured SnO_2	220	100	55	[36]
SnO_2 nanoparticles	N/A	100	74	This work

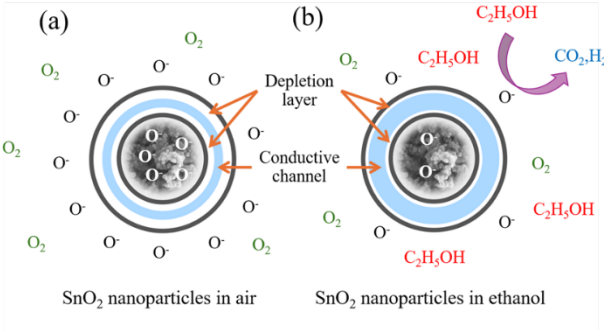

Figure 11. Schematic representations of the electrical configurations of SnO_2 nanoparticles in (a) air, and (b) ethanol environments, respectively.

The superior performance of this sensor is attributed to the optimized SnO_2 sensing layer thickness (0.71 µm), which enhances gas adsorption while ensuring efficient electron transport. The porous structure of the SnO_2 nanoparticle layer provides sensitivity comparable to more complex nanostructures, while using a low-voltage LTCC micro hotplate significantly reduces energy requirements. These features make the sensor a highly practical solution for ethanol detection in portable, IoT-enabled, and energy-constrained applications.

4. Conclusion

This study investigated the development and optimization of SnO_2-based gas sensors integrated with a low-temperature co-fired ceramic (LTCC) micro hotplate. Sensors with varying layer thicknesses (0.24 µm, 0.71 µm, and 1.20 µm) were prepared to examine the impact of thickness on gas detection performance. The findings indicate that the 0.71 µm layer provides the best balance between high sensitivity, fast response, and efficient recovery, making it the optimal configuration for ethanol detection. The porous structure of the SnO_2 layer enhances gas adsorption, while maintaining good electron mobility, ensuring reliable performance with minimal power consumption. The sensor demonstrates strong potential for low-power applications such as portable and battery-operated devices. Additionally, due to favorable surface interactions and reaction kinetics with ethanol molecules, the sensor showed superior selectivity for ethanol compared to other VOCs like hydrogen sulfide, ammonia, acetone, and nitric oxide.

Although the sensor performed well, several improvements could further enhance its capabilities. Future work could explore doping SnO_2 with metals or composite materials to boost sensitivity and selectivity, develop multi-layer designs for multi-gas detection, and investigate the effects of temperature control for performance optimization under fluctuating environmental conditions. Further studies on long-term stability and miniaturization could extend the sensor's practical use for wearable devices and IoT-based monitoring systems. In summary, the low-power, highly selective SnO_2 sensor developed in this study offers promising potential in ethanol detection, industrial safety, environmental monitoring, and medical diagnostics.

Acknowledgements

The author would like to thank the Faculty of Science, Silpakorn University, Nakhon Pathom, Thailand, for financial support (Grant No. SRIF-JRG-2565-09).

References

[1] R. Kumar, A. Kumar, R. Singh, R. Kashyap, R. Kumar, D. Kumar, S. K. Sharma, and M. Kumar, "Room temperature ammonia gas sensor using Meta Toluic acid functionalized graphene oxide," *Materials Chemistry and Physics,* vol. 240, p. 121922, 2020.

[2] M. Nami, M. Taheri, I. A. Deen, M. Packirisamy, and M. J. Deen, "Nanomaterials in chemiresistive and potentiometric gas sensors for intelligent food packaging," *TrAC Trends in Analytical Chemistry,* p. 117664, 2024.

[3] S. Dhall, B. Mehta, A. Tyagi, and K. Sood, "A review on environmental gas sensors: Materials and technologies," *Sensors International,* vol. 2, p. 100116, 2021.

[4] J. Luo, T. Dziubla, and R. Eitel, "A low temperature co-fired ceramic based microfluidic Clark-type oxygen sensor for real-time oxygen sensing," *Sensors and Actuators B: Chemical,* vol. 240, pp. 392-397, 2017.

[5] C. W. Ji, J. D. Mun, C. B. Yoon, and H. C. Lee, "Low temperature co-fired ceramic-based and heater-embedded toxic gas sensors with nanostructured SnO_2 thick films," *Journal of Nanoscience and Nanotechnology,* vol. 19, no. 8, pp. 5227-5232, 2019.

[6] L. Kulhari, K. Ray, N. Suri, and P. Khanna, "Detection and characterization of CO gas using LTCC micro-hotplates," *Sadhana,* vol. 45, pp. 1-6, 2020.

[7] Y. Shen, W. Wang, A. Fan, D. Wei, W. Liu, C. Han, Y. Shen, D. Meng, and X. San, "Highly sensitive hydrogen sensors based on SnO_2 nanomaterials with different morphologies," *International journal of hydrogen energy,* vol. 40, no. 45, pp. 15773-15779, 2015.

[8] A. K. Mauraya, P. Singh, S. Muthiah, S. S. Kushvaha, and S. K. Muthusamy, "Effect of post-oxidation processes and thickness of SnO_2 films prepared by vacuum evaporation on

CO gas sensing characteristics," *Ceramics International,* vol. 47, no. 9, pp. 13015-13022, 2021.

[9] W. Yuan, K. Yang, H. Peng, F. Li, and F. Yin, "A flexible VOCs sensor based on a 3D Mxene framework with a high sensing performance," *Journal of Materials Chemistry A,* vol. 6, no. 37, pp. 18116-18124, 2018.

[10] S. Ying, Y. Wang, Z, Wu, M. Huang, L. Dong, J. Zhao, and C. Peng, "Highly-sensitive NO_2 gas sensors based on three-dimensional nanotube graphene and ZnO nanospheres nano-composite at room temperature," *Applied Surface Science,* vol. 566, p. 150720, 2021.

[11] M. A. Franco, P. P. Conti, R. S. Andre, and D. S. Correa, "A review on chemiresistive ZnO gas sensors," *Sensors and Actuators Reports,* vol. 4, p. 100100, 2022.

[12] V. Kumar, A. Singh, B. C. Yadav, H. K. Singh, D. P. Singh, S. K. Singh, and N. Chaurasiya, "Environment-sensitive and fast room temperature CO_2 gas sensor based on ZnO, NiO and Ni-ZnO nanocomposite materials," *Environmental Functional Materials,* vol. 2, no. 2, pp. 167-177, 2023.

[13] A. Rydosz, W. Maziarz, T. Pisarkiewicz, H. B. de Torres, and J. Mueller, "Thermal and electrical investigation on LTCC gas sensor substrates," *International Journal of Information and Electronics Engineering,* vol. 6, no. 3, pp. 143-146, 2016.

[14] N. Ababii, M. Hoppe, S. Shree, A. Vahl, M. Ulfa, T. Pauporte, B. Viana, V. Cretu, N. Magariu, V. Postica, V. Sontea, M.-I. Terasa, O. Polonskyi, F. Faupel, R. Adelung, and O. Luopan, "Effect of noble metal functionalization and film thickness on sensing properties of sprayed TiO_2 ultra-thin films," *Sensors and Actuators A: Physical,* vol. 293, pp. 242-258, 2019.

[15] Z. Li, A. A. Haidry, T. Plecenik, M. Vidis, B. Grancic, T. Roch, M. Gregor, P. Durina, Z. Yao, and A. Plecenik, "Influence of nanoscale TiO_2 film thickness on gas sensing properties of capacitor-like Pt/TiO_2/Pt sensing structure," *Applied Surface Science,* vol. 499, p. 143909, 2020.

[16] R. Paulraj, P. Ramasamy, and N. Vijayan, "One step synthesis of tin oxide nanomaterials and their sintering effect in dye degrdation," *Optik,* vol. 135, pp. 434-445, 2017.

[17] N. Horti, M. Kamatagi, N. Patil, M. Wari, and S. Inamdar, "Photoluminescence properties of SnO_2 nanoparticles: effect of solvents," *Optik,* vol. 169, pp. 314-320, 2018.

[18] K. Jaruwongrungsee, "Gas sensing device, its fabrication and signal analysis process thereof," Thailand Patent 2301005878, 2023.

[19] Y. K. Gautam, K. Sharma, S. Tyagi, A. K. Ambedkar, M. Chaudhary, and B. Pal Singh, "Nanostructured metal oxide semiconductor-based sensors for greenhouse gas detection: Progress and challenges," *Royal Society open science,* vol. 8, no. 3, p. 201324, 2021.

[20] A. N. Kawade, P. K. Bhujbal, A. T. Supekar, H. M. Pathan, and K. M. Sonawane, "Eosin-Y sensitized tin oxide (SnO_2): Fabrication and its analysis," *Optik,* vol. 216, p. 164968, 2020.

[21] Y. Masuda, "Recent advances in SnO_2 nanostructure based gas sensors," *Sensors and Actuators B: Chemical,* vol. 364, p. 131876, 2022.

[22] M. Honarmand, M. Golmohammadi, and A. Naeimi, "Bio-synthesis of tin oxide (SnO_2) nanoparticles using jujube fruit for photo-catalytic degradation of organic dyes," *Advanced Powder Technology,* vol. 30, no. 8, pp. 1551-1557, 2019.

[23] G. Jozanikohan and M. N. Abarghooei, "The Fourier transform infrared spectroscopy (FTIR) analysis for the clay mineralogy studies in a clastic reservoir," *Journal of Petroleum Exploration and Production Technology,* vol. 12, no. 8, pp. 2093-2106, 2022.

[24] P. Luque, H. E. Garrafa-Galvez, O. Nava, A. Olivas, M. E. Martinez-Rosas, A. R. Vilchis-Nestor, A. Villegas-Fuentes, and M. J. Chinchillas-Chinchillas,"Efficient sunlight and UV photo-catalytic degradation of methyl orange, methylene blue and Rhodamine B, using Citrus×paradisi synthesized SnO_2 semi-conductor nanoparticles," *Ceramics International,* vol. 47, no. 17, pp. 23861-23874, 2021.

[25] J. Huang, L. Wang, C. Gu, Z. Wang, Y. Sun, and J.-J. Shim, "Preparation of porous SnO_2 microcubes and their enhanced gas-sensing property," *Sensors and Actuators B: Chemical,* vol. 207, pp. 782-790, 2015.

[26] Z. Song, S. Xu, M. Li, W. Zhang, H. Yu, Y. Wang, and H. Liu, "Solution-processed SnO_2 nanowires for sensitive and fast-response H_2S detection," *Thin Solid Films,* vol. 618, pp. 232-237, 2016.

[27] I. Khan, Z. H. Yamani, and A. Qurashi, "Sonochemical-driven ultrafast facile synthesis of SnO_2 nanoparticles: growth mechanism structural electrical and hydrogen gas sensing properties," *Ultrasonics sonochemistry,* vol. 34, pp. 484-490, 2017.

[28] M. A. Han, H.-J. Kim, H. C. Lee, J.-S. Park, and H.-N. Lee, "Effects of porosity and particle size on the gas sensing properties of SnO_2 films," *Applied Surface Science,* vol. 481, pp. 133-137, 2019.

[29] Y. Sun, J. Guo, J. Qi, B. Liu, and T. Yu, "Comparisons of SnO_2 gas sensor degradation under elevated storage and working conditions," *Microelectronics Reliability,* vol. 114, p. 113808, 2020.

[30] Z. Cai, E. Goo, and S. Park, "Synthesis of tin dioxide (SnO_2) hollow nanospheres and its ethanol-sensing performance augmented by gold nanoparticle decoration," *Journal of Alloys and Compounds,* vol. 883, p. 160868, 2021.

[31] X. Ma, H. Song, and C. Guan, "Enhanced ethanol sensing properties of ZnO-doped porous SnO_2 hollow nanospheres," *Sensors and Actuators B: Chemical,* vol. 188, pp. 193-199, 2013.

[32] Y. Zhao, J. Liu, Q. Liu, Y. Sun, D. Song, W. Yang, J. Wang, and L. Liu, "One-step synthesis of SnO_2 hollow microspheres and its gas sensing properties," *Materials Letters,* vol. 136, pp. 286-288, 2014.

[33] C. A. Zito, T. M. Perfecto, and D. P. Volanti, "Impact of reduced graphene oxide on the ethanol sensing performance of hollow SnO_2 nanoparticles under humid atmosphere," *Sensors and Actuators B: Chemical,* vol. 244, pp. 466-474, 2017.

[34] B. Wang, L. Sun, and Y. Wang, "Template-free synthesis of nano-sheets-assembled SnO_2 hollow spheres for enhanced ethanol gas sensing," *Materials Letters,* vol. 218, pp. 290-294, 2018.

[35] Z. Yuan, K. Zuo, F. Meng, Z. Ma, W. Xu, and H. Dong, "Microscale analysis and gas sensing characteristics based on SnO_2 hollow spheres," *Microelectronic Engineering,* vol. 231, p. 111372, 2020.

[36] Y. Zhao, Y. Liu, Y. Ma, Y. Li, J. Zhang, X. Ren, C. Li, J. Zhao, J. Zhu, and H. Zhao, "Hollow pentagonal-cone-structured SnO_2 architectures assembled with nanorod arrays for low-temperature ethanol sensing," *ACS Applied Nano Materials,* vol. 3, no. 8, pp. 7720-7731, 2020..